JATIS Journal of Astronomical Telescopes, Instruments, and Systems

RESEARCH PAPER

Facility for the radiometric characterization of space-based visible-near infrared detectors

Miriam E. Cisneros-González,[a,b,*] David Bolsée,[b,*] Nuno Pereira,[b] Lionel Van Laeken,[b] Lars Jacobs,[b] Ann Carine Vandaele,[b] Özgür Karatekin,[c] Clément Lauzin,[a] and Séverine Robert[b]

[a]Université catholique de Louvain, Institute of Condensed Matter and Nanosciences, Louvain-la-Neuve, Belgium

[b]Royal Belgian Institute for Space Aeronomy, Brussels, Belgium

[c]Royal Observatory of Belgium, Brussels, Belgium

ABSTRACT. When developing new astronomical instruments, there is a need to perform the characterization of their individual components, especially the detectors, to ensure that their performances comply with the scientific objectives of the instrument. A visible-near infrared (VIS-NIR) facility was developed for the absolute and relative radiometric characterization of space-based detectors at the Royal Belgian Institute for Space Aeronomy (BIRA-IASB). The facility operates from 0.4 to 2.65 μm in an ISO-5 environment. It offers a tunable monochromatic flux with a high level of straylight rejection (10^{-8}) and 2% uniformity, over a four-decade range of intensity with adjustable bandwidth. Latency measurements are also possible. Thermalization is offered within a precision of 7 mK between 50 K and 382 K. The ultimate vacuum level of the detector chamber is below 10^{-6} mbar. A robust security system avoids both reaching temperatures outside the operational range of the detector and its electronics, and contamination due to vacuum loss. The facility was already used to characterize the VIS-NIR detectors of the Moons And Jupiter Imaging Spectrometer (MAJIS), one of the instruments on board the Jupiter ICy Moons Explorer (JUICE). The versatility provided by the VIS-NIR facility allows its use for the characterization of other astronomical detectors.

 [DOI: 10.1117/1.JATIS.9.3.036001]

Keywords: VIS-NIR detectors; absolute radiometry; quantum efficiency; test facility; detectors characterization; space-based detectors

Paper 23042G received Apr. 6, 2023; revised Jun. 23, 2023; accepted Jul. 11, 2023; published Aug. 1, 2023.

1 Introduction

The need to characterize imaging detectors is essential to confirm their performances for both space- and ground-based instruments, since often the characterization offered by the manufacturers does not meet the stringent accuracy requirements for scientific instruments. Besides, numerical simulations are vulnerable to conceptual and implementation errors because of the limited understanding of the detector's physics, and the development of data analysis methods to reduce the undesirable detector characteristics can take years.[1] For imaging, the understanding of the behavior and performances of each pixel under different illumination conditions, wavelengths, and temperatures must be accurately evaluated, considering the potential environment to which a detector could be exposed. For instance, depending on their operational spectral range,

*Address all correspondence to Miriam E. Cisneros-González, miriam.cisneros@uclouvain.be; David Bolsée, david.bolsee@aeronomie.be

detectors usually require cryogenic operating conditions to reduce the thermal noise generated during image acquisition, especially infrared (IR) detectors. However, if the thermal control is limited, it might be possible that during observations the nominal temperature of the detector varies, which will directly affect the signal-to-noise ratio (SNR) of the images. In addition, detectors onboard space missions are subjected to harsh radiation environments, and therefore their performances downgrade with time.[2,3] Hence, to fully understand the instrument and its response over time, to assess the evolution of its performances during observations, the initial measured characteristics of the detector will be the crucial starting reference point for any subsequent analysis.[4]

Due to the complexity of characterization procedures, according to Shapiro et al.,[1] the resultant measured performances of a detector could bias photometric, astrometric, spectroscopic, and shape measurements at the 1% level or less. However, if a detector is well characterized by providing the different conditions to which it will be exposed during operation, including the expected image acquisition methods, there will be enough confidence that the detector will perform according to its specifications in all feasible environments, including critical performance parameters.[5] The required optical sources, data acquisition methods, and minimum specifications for both test chambers and optical systems can be derived from the specific planning of measurements[6] and, for maintaining repeatability, it is desirable to have as simple as an optical system can be.[5,7]

1.1 Typical Characterization Measurements

Traditionally, many detector parameters, such as responsivity and noise, are measured by exposing the detector to a spatially uniform photon flux or dark conditions, respectively.[8] The photon flux uniformity can be achieved by means of a diffuser or an integrating sphere (IS), although these devices will highly reduce the irradiance at the detector, and special considerations must be taken into account to still provide enough signal to it. The irradiance must be stable, homogeneous, and with a well-known spectral response covering the operating spectral range of the detector to be characterized, and this can only be confirmed by a proper characterization of the sensitive area of the detector, i.e., the optical working plane (WP).

On the other hand, parameters such as quantum efficiency (QE) and spectral response, which are highly wavelength dependent, require a monochromatic light source to illuminate the detector at the desired wavelength with high spectral purity. Normally for these measurements, the current of a reference calibrated photodiode is measured first to determine the irradiance received at the WP of the optical setup for a certain illumination. In this way, when exposing the detector to be characterized under the same illumination and exactly at the same position as the reference photodiode, it is possible to determine how many of those photons produced signal in each of the pixels of the detector.[6] Therefore, the accuracy of the measurement will be depending on the stability of the light source and the alignment of the detector. The monochromatic light source can be either obtained from different light-emitting diode (LED) sources or lasers or through the combination of a continuum light source, such as lamps or blackbodies, and a monochromator.

Another parameter relevant to the characterization of a light detector is its linearity. Although it is expected that a detector responds linearly with incident light, this linearity is often deviated depending mainly on the transimpedance of the metal-oxidesemiconductor field-effect transistor (MOSFET) amplifiers of the detector array.[6] When measuring linearity, the detector should generate signal from its minimum level to saturation. This can be done by exposing the detector to different incident radiation while acquiring images with the same integration time (linearity versus flux) or by providing constant incident radiation while acquiring images at different integration times (linearity versus integration time). Measuring linearity at a constant photon flux depends also on the stability and homogeneity of the light source to guarantee that each pixel is exposed to the same amount of photons during the complete measurements.

Because background measurements are an important part of the image acquisition procedure, a characterization facility must include a shutter in which the light source can be stopped, so that any emission produced by devices along the optical path can be subtracted from the measurements during data processing. This is also related to the measurement of the persistence effect, which is related to the residual signal in a pixel after a bright exposure. Therefore, the

speed of the shutter must be synchronized with the integration time of the detector during data acquisition.

Finally, measuring parameters that do not require the illumination of the detector, such as dark current (DC) and read-out noise, requires removing emissions from surrounding bodies at the wavelengths at which the detector is sensitive. For instance, an IR detector is generally enclosed by radiation shields at cryogenic temperatures, so the blackbody emission from bodies at room temperature is blocked, whereas the radiation from the cold shield does not produce any background signal in the detector. Therefore, these measurements will be accurate if the dark conditions are guaranteed and if the detector is at a stable temperature.

When measuring non-uniformities, as is the case for dark signal non-uniformity and photo response non-uniformity, the spatial differences between pixels are analyzed. In consequence, there is no need to use reference photodiodes during the measurements. These non-uniformities are due to imperfections during the fabrication process of the detector, which provides different values of capacitance.[6]

In the end, the accurate determination of the performance parameters of any imaging detector is a challenge that could be tackled if a single, but versatile characterization facility is used.[6]

1.2 VIS-NIR Characterization Facilities Available

Some visible-near infrared (VIS-NIR) facilities are available for the characterization of astronomical detectors. In the case of the European Space Agency (ESA), even if instruments are provided by external consortia, ESA takes responsibility for the procurement of the detectors[9] and can provide infrastructure for their commissioning through ISO-17025 accredited facilities for charged-coupled device (CCD) and complementary metal-oxide-semiconductor (CMOS) detectors' validation.[10] Similarly, the National Aeronautics and Space Administration (NASA), through the Detector Characterization Laboratory, supports flight qualification testing of detectors and detector systems, providing a full optical and electrical characterization of detector arrays.[11] However, usually these facilities are state-of-the-art instruments developed to fulfill the needs of each project (often for also state-of-the-art detectors) to comply with the specifications demanded for each required measurement. This was the case for the Euclid mission,[12,13] the James Webb Space Telescope (JWST),[14–16] and the Large Synoptic Survey Telescope,[17] to mention some examples.

What is typical among these testing facilities is the use of quartz-tungsten-halogen (QTH) and xenon lamps as their main light source. The stability of the lamp is continuously monitored and reported to be in the order of 1%.[18,19] However, the power is not usually higher than 500 W,[20,21] and some considerations must be taken into account to provide enough flux to the detector, especially when the system requires the use of an IS or a diffuser. Other light sources used include 3000 K blackbodies[14,19] and LED illumination sources.[13,16,19] To reach the same level of intensity stability of QTH lamps with LEDs, the temperature of the LED must be stabilized within 300 mK.[13] As LEDs offer illumination at specific wavelengths, it could be possible to disregard the use of a monochromator. This was the case for the Teledyne Imaging Sensors Test Facility.[16] Naturally, if one single facility provides different illumination sources, the optical layout must be reconfigured.

ISs are the general solution to provide a uniform light beam to the detector, especially when measuring QE. However, depending on its properties, some additional items could be added to achieve the desired homogeneity (usually 1%[18]). For instance, when the IS is too small and the image of the aperture is still visible at the output port, adding flat diffusers could improve the uniformity of the beam[22] regardless attenuation. Another solution is to place the detector far from the output of the IS under a baffle system that also reduces straylight.[4,21–23] Neutral-density (ND) filters are also used to vary the light flux of the system,[24–26] although other alternatives, such as diaphragms, apertures, or pinholes of different sizes, have also been adopted,[16,18] sometimes in combination with ND filters.[22,27]

Operating CCD or CMOS detectors at near-infrared (NIR) and even visible wavelengths require their thermalization at cryogenic temperatures. Open-cycle cryostats are used in some characterization facilities[20,21,28] to reach these temperatures. Vibrations in such systems would only come from the pumping system, which is normally disabled during measurements. However, most of the facilities count with closed-cycle cryostats, which are chosen depending

on their power capabilities. For instance, the facilities used for the characterization of the NIR spectrograph detectors for the JWST[16] needed two-stage cold heads: one stage for thermalizing the detectors with independent thermal controls for their electronics, and one stage for thermalizing the optics of the facility. Typical thermal stability provided by the characterization facilities is in the order of millikelvin with temperature rates below 1 K/min.[13,22,29]

It is worth mentioning that working with flight detectors requires that the test facilities are installed inside ISO-5 areas to comply with the necessary cleanliness levels when manipulating space-based detectors. These areas include a robust security system to protect the detectors during the measurements. Considering the additional challenges of supplying (1) uniform flux stability tunable over a large spectral range and (2) a cryogenic environment, using a single versatile test bench to perform absolute and relative radiometric measurements of an imaging detector, is desirable for optimizing resources, time-saving during the measurements, and repeatability of measurement conditions. Therefore, providing a testbench that is flexible, accurate, and highly automated while minimizing the need for customized designs is the main objective of this work. In this paper, a new VIS-NIR characterization facility from the Royal Belgian Institute for Space Aeronomy (BIRA-IASB) is described. This facility has been already used to characterize the VIS-NIR detectors of the Moons And Jupiter Imaging Spectrometer (MAJIS),[30,31] one of the instruments on board the Jupiter ICy Moons Explorer (JUICE). This facility is offered to the scientific community as another option for future projects and contributions.

2 VIS-NIR Characterization Facility at BIRA-IASB

The BIRA-IASB characterization facility follows the requirements specified by the European Space Components Coordination (ESCC)[32] and the European Machine Vision Association (EMVA)[33] current standards for the characterization of imaging detectors. The facility is under a laminar flux certified as an ISO-5 area that includes the optical setup, the thermal-vacuum chamber, and a horizontal laminar flux allocating a working area dedicated to the manipulation of equipment (Fig. 1). The soft-walls are made of anti-static transparent vinyl to allow low outgassing and isolate the ISO-5 area from the gray room, which achieves an ISO-7 cleanliness level. Environmental temperature, pressure, and relative humidity are continuously monitored in both areas. The temperature and relative humidity can be actively controlled to remain at 22°C±3°C and 40% to 65%, respectively. The ground-support equipment (GSE) is located in an ISO-8 area, from which the remote control of devices operating in the clean room is possible.

The facility was designed to measure the parameters listed in Fig. 2. Note that some parameters can be derived from the results of other measurements. Moreover, different illuminating conditions, dynamical illumination levels, temperatures, and exposure times can be provided, besides absolute radiometry to measure parameters such as QE.

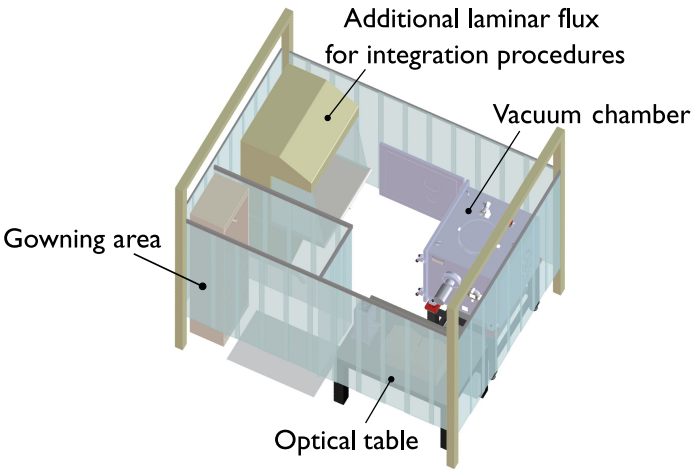

Fig. 1 Schematic diagram of the ISO-5 area where the characterization facility is located.

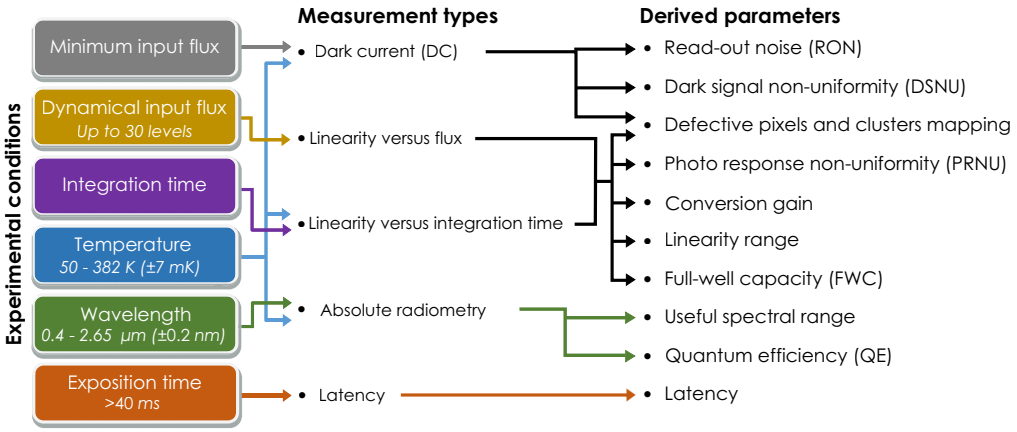

Fig. 2 List of measurements that can be performed with the VIS-NIR characterization facility, and the parameters that can be derived under different experimental conditions, to characterize an imaging detector.

2.1 Cryogenic System

Inside the vacuum chamber, the thermalization of a VIS-NIR detector is made through an oxygen free high-conductivity (OFHC) copper plate on which the detector is installed. The copper plate is thermally connected to the cold finger of the one-stage Advanced Research Systems closed-cycle cryocooler model CS104FT, which provides a cooling power of 60 W at 77 K, with an ultimate performance of 25 K without thermal load. As implemented in the characterization facility, the cold finger can achieve a minimum temperature of 43 K. Both, the cold finger and the copper plate are provided with a proportional-integrative-derivative (PID) thermal control loop. The copper plate counts with a redundant control loop to ensure thermal protection in case of failure of the primary loop. Two LakeShore 335 and one LakeShore 336 temperature controllers are used to regulate the control loops. The copper plate can be stabilized at a temperature between 50 and 382 K, with a difference of 0.01% with respect to the target temperature, and a precision within 7 mK after 2 h of activating the thermal control.

Figure 3 shows a diagram of the high-vacuum system of the BIRA-IASB characterization facility. The vacuum chamber is a customized cubical model with a volume of 420 L. The viewport has a diameter of 63 mm and is made of CaF_2. All O-rings are made of Viton. The pumping equipment consists of a dry primary pump with a pumping speed of 4 L/s, in serial connection with a turbo-molecular pump with 260 L/s of pumping speed that can automatically be activated

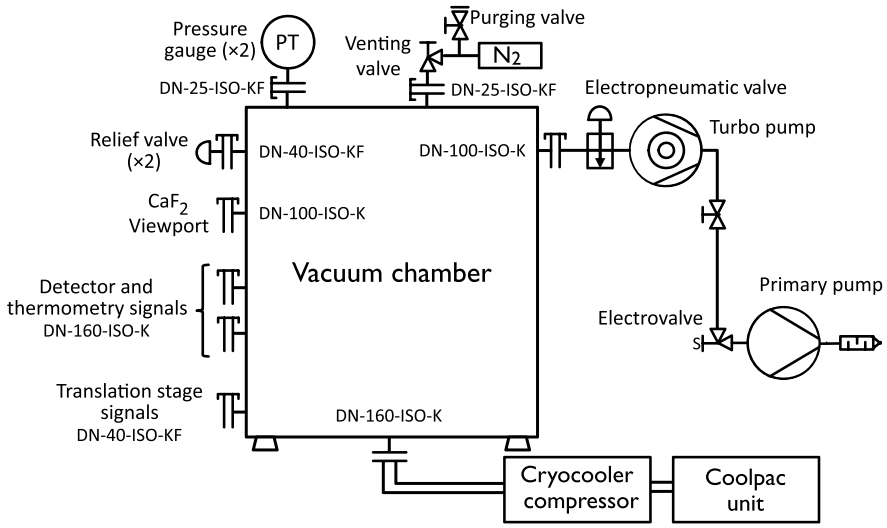

Fig. 3 Schematic diagram of the vacuum system of the VIS-NIR facility. The detector to be characterized would be mounted in front of the CaF_2 viewport inside the vacuum chamber.[34]

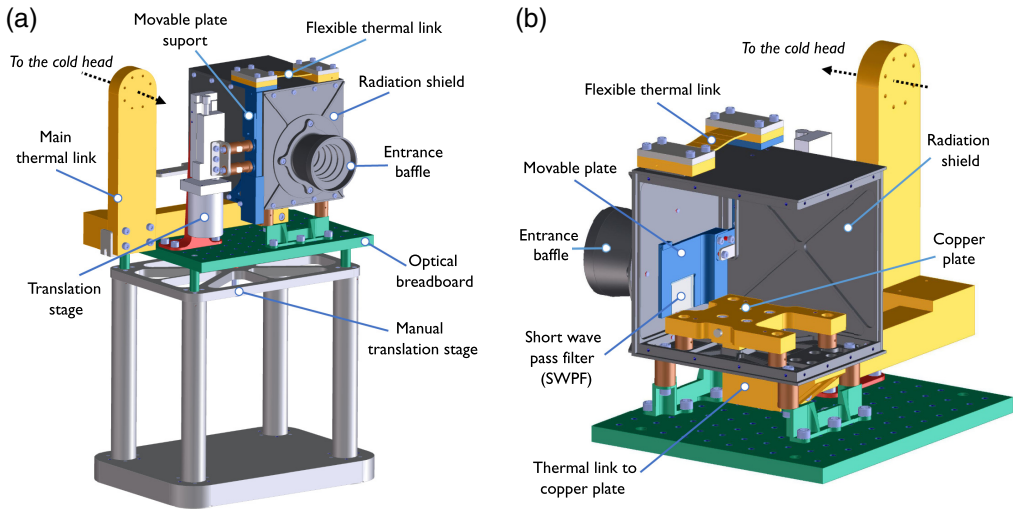

Fig. 4 Mount developed to support and thermalize VIS-NIR detectors: (a) frontal view and (b) internal view of the radiation shield.

when a level of 10^{-1} mbar is achieved inside the chamber. A vacuum level of 10^{-5} mbar is achieved in 80 min, with an ultimate vacuum level of 10^{-7} mbar.[34] An electro-pneumatic valve can isolate the vacuum chamber from the pumping system if needed. The vacuum chamber was designed to keep a high-vacuum level only with the pumping system permanently active. Thanks to the design of the detector mount, vibrations induced by the pumping system and the cryocooler are countered, even during measurements. The venting process is made with ultra-high-purity nitrogen (N5.0).

Figure 4 shows the mount developed to support, thermalize, and optically align the detector in front of the viewport of the vacuum chamber. The four pillars of the base supporting the optical breadboard are part of a translation system for optical alignment in height. Although it is expected that the temperature of the base is always around room temperature, it is thermally isolated from the vacuum chamber by 4 mm thick polytetrafluoroethylene (PTFE) feet (not visible in the figure). The optical breadboard allows the attachment of different components. However, the detector would be installed inside the radiation shield screwed to the copper plate. The room available at the copper plate is limited by the radiation shield to 138.5 mm × 106 mm × 111.5 mm. The focal plane unit, which normally contains the detector and its electronics, should not exceed these dimensions unless a different design is developed for the radiation shield.

The different parts of the mount were carefully designed. The materials used have low outgassing levels, i.e., a total mass lost (TML) lower than 1% and a collected volatile condensable materials (CVCM) lower than 0.1%. The main conductive material used was OFHC copper, whereas PEI-Ultem™ 1000 was chosen as the main insulating material due to its low thermal conductivity (0.24 $W\,m^{-1}\,K^{-1}$).[35] Indium foils were used between different mechanical interfaces to improve thermal conductivity when necessary.

It is worth mentioning that 15 PT100 resistance temperature detectors are installed at the key parts of the mount. In total, the facility offers the possibility of monitoring the temperature of up to 24 locations, from which 6 can be part of a temperature control loop. NI data acquisition modules are used for temperature monitoring besides the LakeShore controllers. The monitoring of critical parts, such as the copper plate and the movable plate, is performed through calibrated temperature sensors and might be redundant. Thermometry is wired by the fourth-lead technique to eliminate the effect of lead resistance on the measurement of the temperature sensors. The systematic error of the temperature measurements varies from 22 to 79 mK, depending on temperature.

In terms of safety, the thermal GSE (TGSE) is continuously monitoring the temperature sensors and the user can configure different alarms to protect sensitive devices from temperatures outside their operating range, including the detector to be characterized. Therefore, if the temperature is too low to compromise the functioning of the detector, the cryocooler is deactivated

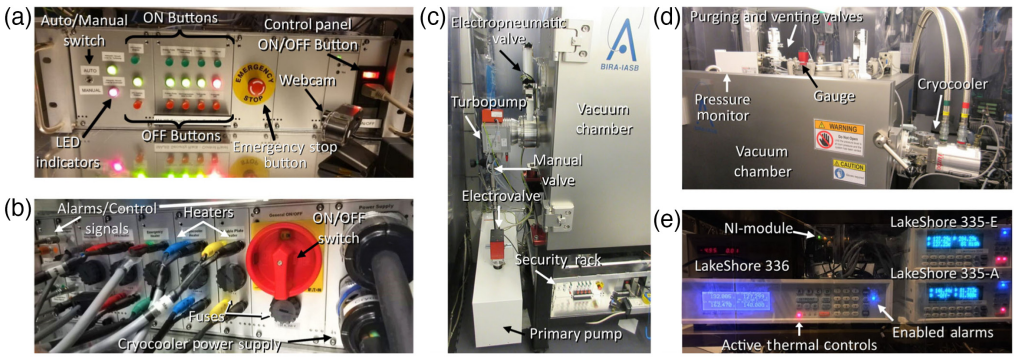

Fig. 5 Security system components[36]: (a) control panel of the security rack, (b) rear panel of the security rack, (c) pumping system, (d) cryocooler and pressure gauge, and (e) temperature monitors and controllers.

automatically, and if the temperature is too high (usually during warming up or outgassing processes), the concerned heaters are deactivated. The temperature rate of the copper plate when suddenly disconnecting the cryocooler is not higher than 0.5 K/ min. Similarly, the TGSE is continuously monitoring the vacuum level in the chamber through a pressure gauge with 30% of accuracy between 1×10^{-9} and 1×10^{3} mbar. A redundant pressure gauge is available in case of failure of the main one. The TGSE was developed in LabVIEW with some functionalities in Python. The data acquired during the campaign of measurements is backed up in the servers of BIRA-IASB, including detector frames, radiometry, thermometry, and ambient parameters. Moreover, backup computers can substitute the optical and the TGSE systems in case of failure.

The core of the security system is a security rack whose control panel is available from the clean room although the main functionalities can be accessed from the TGSE. The TGSE controls temperature and pressure monitors while displaying and registering data in real time. Together with the pumping system, the TGSE provides the input conditions to the security rack for the activation or deactivation of the different devices of the cryogenic system. If any anomaly is detected, such as failures in the pumping system or leaks, the electro-pneumatic valve is automatically closed to avoid vacuum loss. In addition, an electrovalve is available to isolate the turbo-molecular pump from the primary pump. Overpressure is avoided by means of pressure relief valves installed in the vacuum chamber to mainly protect the viewport during the venting process. In case of a power blackout, the cryogenic system will stop working and the electro-pneumatic valve will close. However, an uninterruptible power supply system is available to continue powering the TGSE for the monitoring of pressure and temperature conditions for 4.5 h after the power blackout. In case of a general power blackout, BIRA-IASB counts with an electricity generator with the capability to supply energy to the institute for ~24 h during working days, or up to ~48 h during weekends. Moreover, the control panel of the security rack includes an emergency stop button to immediately suspend the functioning of the pumping and cryogenic systems while the electro-pneumatic valve of the vacuum chamber is closed, without compromising the safety of the sensitive devices installed inside the vacuum chamber. If an irregularity is detected, SMS messages notify the operators in charge. This is especially useful during nights and weekends. Additional details concerning the security system of the VIS-NIR characterization facility can be consulted in Ref. 36. Figure 5 shows pictures of the security rack and the vacuum system of the VIS-NIR characterization facility.

2.2 Optical System

To perform measurements in dark conditions, the VIS-NIR detector to be characterized must be harbored inside a closed radiation shield designed to limit its own thermal contribution and block the straylight from warm objects around it. Considering a threshold for negligible background radiation of 1 e^{-} s^{-1} pix^{-1} for a VIS-NIR detector with a spectral cut-off at 2.5 μm, the radiation shield must be kept at a temperature below 172 K.[37] From validation tests (Sec. 3.1), it was probed that the radiation shield of the BIRA-IASB facility is ~10 K warmer than the cold plate when thermalizing a detector at nominal temperature (132 K), well below the limit of 172 K.

The radiation shield of the facility is black anodized to reduce internal reflections, and it is externally covered with multi-layer insulation (MLI) jackets to reflect back radiation from surrounding objects. However, the radiation shield is not completely closed; it was designed to allow the photon flux entrance from the viewport of the vacuum chamber to perform measurements at light conditions when required. For this purpose, the mount was provided with the Standa vacuum-compatible motorized translation stage model 8MT30V-50, which allows the opening and closing of the radiation shield by a movable plate. An optical filter was added to the movable plate to reject the thermal radiation of the viewport for wavelengths larger than 1.47 μm. If required, the movable plate can also be thermalized through a PID temperature control loop, although the minimum temperature achievable will depend on the temperature of the radiation shield. The movable plate is 13 K warmer than the radiation shield (see Sec. 3.1), so it will approach the limit of 172 K only when the cold plate has a temperature of 157 K, which would correspond to a temperature already outside the typical range to thermalize a VIS-NIR detector for testing. Therefore, the thermal radiation produced by the radiation shield (and movable plate) on an H1RG™ detector array of 1024×1024 pixels is estimated as 5.8×10^{-3} $e^- s^{-1} pix^{-1}$ for the nominal case (132 K) and 6.5×10^{-2} $e^- s^{-1} pix^{-1}$ for the hottest case (144 K). These values are slightly different from what is reported in Bolsée et al.[34] due to the improvements performed to reduce straylight since then (see Sec. 3.2).

Figure 6 shows a schematic diagram of the optical design of the VIS-NIR facility. To let light reach the detector, the movable plate is kept either open or at the filter position. The photon flux is produced by a 1000 W QTH lamp covering the working range from 0.4 to 2.65 μm. The lamp is operated in continuous current mode with 8 A $\pm$ 80 μA, resulting in radiance stability ~0.1%.[34] The stability of the lamp is continuously monitored by a VIS-NIR four-channel filter radiometer with ~10 nm of bandwidth (BW). An infrasil condenser and focusing lens collimate the beam

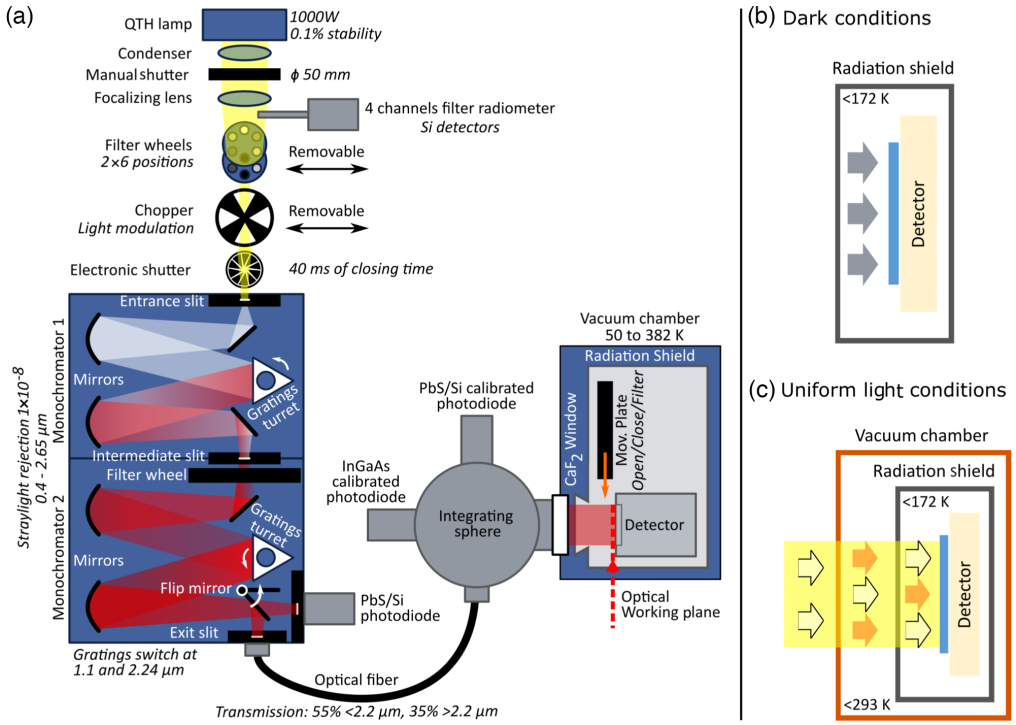

Fig. 6 Optical diagram of the VIS-NIR characterization facility and equivalence models: (a) wavelength injection and signal monitoring from the QTH lamp to the detector inside the vacuum chamber; (b) radiation model when the movable plate of the radiation shield is closed, providing dark conditions to the detector as if a blackbody surrounded it at a temperature below 172 K; (c) radiation model when the movable plate of the radiation shield is opened, the detector receives the light flux from the output of the IS besides the thermal radiation from the CaF_2 window at room temperature. When the movable plate of the radiation shield is at the filter position, the thermal radiation from room temperature bodies is removed.

from the lamp to focalize it in the entrance slit of a double-monochromator. The DTMc300 Bentham double-monochromator provides a monochromatic and tunable photon flux, with up to 10^{-8} straylight rejection. The diffraction gratings implemented in each monochromator are optimized for the VIS-NIR spectral range between 0.4 and 3.5 μm, with an accuracy on the wavelength scale of ± 0.1 nm up to 1.1 μm, and ± 0.25 nm for longer wavelengths. The wavelength selection by the monochromator can be remotely controlled from the GSE room. The only element that must be manually adjusted is the slit width to tune the bandpass for each monochromator.

The output of the double-monochromator is coupled to a 4-port IS of 13.5 cm in diameter through a 1 m long optical fiber. The optical fiber has an average transmission of 48% and wavelength cut-off around 2.65 μm. As it is configured, the monochromator could be used for wavelengths up to 3.5 μm if the optical fiber is replaced.

The IS is coated with spectralon (PTFE) material, suitable for VIS-NIR wavelengths. The output port of 6.35 cm in diameter is placed at the viewport of the vacuum chamber to transfer the high-homogeneity radiance to the detector. The use of absolute calibrated photodiodes in the additional ports of the IS allows for performing absolute radiometric measurements with the characterization facility, besides monitoring the stability of the signal in real-time during measurements. For this purpose, an experimental transfer function was obtained to determine the ratio of the spectral power available in one reference point of the optical WP and its corresponding point in the reference port of the IS for each wavelength (see Sec. 3.2). The inhomogeneity in the illumination intensity provided by the IS at the WP and its spectral dependence were also characterized and allowed the application of a corrective factor to calculate the optical power at any position of the WP. Therefore, the optical alignment of the IS and the detector is critical.

The IS is aligned to the viewport of the vacuum chamber by means of a mechanical interface that also reduces straylight. On the other side of the viewport, the detector is aligned with respect to the baffle of the radiation shield in the optical WP of the facility in such a way that it is possible to determine which pixel of the detector intersects the central axis of the viewport. If the detector is well aligned, then the calibration can be used for absolute radiometry for each pixel.

Performing relative radiometry is simpler. The radiance at the detector must be stable during measurements, which can be demonstrated by monitoring the photodiodes at the IS. The calibration of illumination levels for measurements, such as linearity in function of flux, can also be performed through the monitoring of the reference photodiodes. The photodiodes used include a Bentham Si detector for wavelengths shorter than 1 μm, and a Bentham PbS detector to replace the Si detector for wavelengths longer than 1 μm. The Si photodiode was calibrated by the National Metrology Institute Physikalisch-Technische Bundesanstalt (PTB), and the PbS photodiode was calibrated by Bentham. Light modulation is necessary when the PbS photodiode is in use to optimize its SNR. Then, a removable chopper is placed at the entrance of the monochromator, and a phase-sensitive detection system is used to read its signal. To allow continuous monitoring of the signal between 0.5 and 2.35 μm, a Hamamatsu InGaAs photodiode is additionally included to stay operational when the chopper is removed to illuminate the detector without phase-sensitive detection. Additional photodiodes can be installed at the dual output of the monochromator for signal monitoring.

The facility can provide up to 30 different levels of attenuation over four orders of magnitude through the combination of several ND filters located in two filter wheels after the light source.[34] To stop any light exposure in the detector, the facility includes the electronic Uniblitz shutter DSS335B at the entrance slit of the monochromator. Since it has a maximum closing time of 40 ms, it can be used for latency measurements.

It is worth mentioning that the optical path between the monochromator and the external side of the viewport of the vacuum chamber is continuously flushed with nitrogen gas to avoid light absorption due to atmospheric water vapor. The Nitrocraft Nitrogen Generator NCS-004C available provides a flow of 0.6 L/min. Special attention was considered to avoid introducing straylight through the pipes.

As it is described, the BIRA-IASB facility to characterize VIS-NIR detectors is versatile enough to allow the measurement of parameters that require dark and uniform light conditions varying dynamical illumination levels and wavelengths, besides the possibility of performing absolute radiometry while stabilizing the detector at different temperatures—all without modifying the main configuration of the facility and allowing the automation of measurements during

the characterization campaigns without compromising the sensitive devices of the facility, thanks to its robust security system. Moreover, the facility is installed in an ISO-5 area that complies with clean environmental conditions continuously monitored, allowing its use for space projects.

3 Subsystems Validation

Before characterizing a flight model (FM) detector, the facility had to be thermally and optically validated to ensure that the capabilities required for a complete characterization of a VIS-NIR detector were met, without compromising the safety of the detector.

3.1 Cryogenic System

The vacuum system was carefully cleaned and degassed as well as every component of the mount was cleaned and baked out above 100°C before the assembly. The filter of the movable plate and the translation stage were installed as provided by the manufacturers, with no need for additional cleaning or baking out.

The design of the mount was initially verified by a thermal analysis performed using the CreoSimulate software before the manufacturing of the parts. However, at this stage, the radiation shield and the movable plate were designed to keep a temperature close to 172 K with the cold head thermalized at 77 K. From the optical validation phase, several shielding modifications were performed at the movable plate, besides the use of a stronger thermal connection between the main thermal link and the radiation shield (Sec. 3.2). As a result, the movable plate and the radiation shield thermalize around 147 and 130 K, respectively, with the cold head at 80 K.

The thermal tests also revealed the impact that the opening of the movable plate has on the internal temperature of the radiation shield. The temperature of the copper plate is not perturbed, thanks to the PID control loop, but this will not be the case for the temperature of a detector that is not directly controlled by a PID loop, as was the case for the MAJIS project. For instance, during the characterization of the MAJIS spare model (SM) detector,[31] the temperature of the movable plate in the open position increased by 9 K and produced a maximum temperature variation on the detector of 1.6 K. Fortunately, even during measurements under light conditions, the movable plate remained below the limit of 172 K and produced a negligible effect on the signal of the detector. However, to compensate for the temperature increase of the detector, the copper plate was thermalized 1.6 K below its nominal temperature. Consequently, after a position change of the movable plate, it is necessary to change the thermalization of the copper plate accordingly and wait at least 2 h for the temperature to stabilize (±0.5 K from target temperature).[38]

The cooling-down and warming-up processes were defined during the validation phase. Figure 7 shows the vacuum and temperature evolution of the cryogenic system with no detector installed in the mount. At least 80 min are needed to achieve a vacuum level from room pressure to below 1×10^{-4} mbar in the vacuum chamber and activate the cryocooler for the cooling down of the mount. About four more hours are needed to stabilize the temperature of the copper plate to

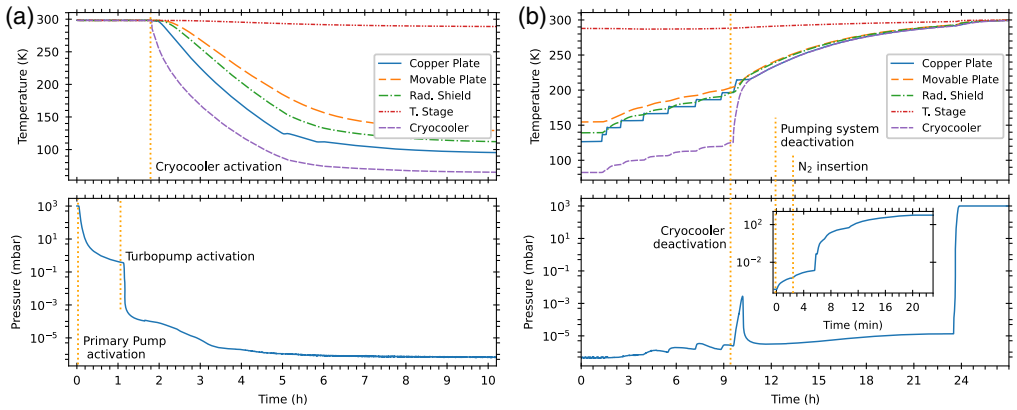

Fig. 7 Performances of the cryogenic system of the characterization facility. (a) Pumping down of the vacuum chamber (bottom) and cooling down of the mount (top). (b) Warming up of the mount (top) and venting of the vacuum chamber (bottom).

its target temperature, with a maximum rate of −0.9 K/min.[34] The temperature rate of the warming-up process is defined by the capabilities of the vacuum system to pump out the outgassing of materials and by the rate at which the detector can be exposed. For instance, the temperature changes for the MAJIS VIS-NIR detectors could not exceed 5 K/min.[36] To avoid molecular contamination on the detector during the warming-up process, the coldest item must never be the detector itself. So depending on the temperature evolution of the mount and the vacuum level of the chamber, the cryocooler could be deactivated when the detector is above 200 K.[34] Once every item of the mount is at room temperature, the vacuum system can be stopped and the venting process can be performed.

To validate the security system, it was necessary to produce the conditions that would cause the system to fail. No real detector was installed in the facility during these tests, but two additional temperature sensors were installed in the copper plate to reproduce the thermometry signals of the detector itself and its electronics. The tests included: power blackout at different stages of the pumping-out and cooling-down processes, interruption of the operation of the primary pump at different vacuum regimes, interruption of the operation of the cryocooler, activation of every low- and high-temperature alarm, leak simulation in the vacuum chamber, and activation of the emergency button at different stages of the pumping-out and cooling down processes. The only situation that was not tested during the validation of the security system was overpressure inside the vacuum chamber.

Figure 8 shows the thermal-vacuum behavior of the chamber during the most representative tests. The temperature alarms are activated by considering the thermal inertia of the temperature change due to the deactivation of either the heaters or the cryocooler. Therefore, the corresponding actuator is always deactivated before the real temperature limit of the sensitive device is achieved. For instance, in Fig. 8(a), the copper plate is heated until the temperature measured by detector 2 reaches 318 K; the heaters in the copper plate are deactivated by the security system, and although the temperature continues increasing, detector 2 does not reach the temperature limit defined at 320 K. Similarly in Fig. 8(b), the copper plate is cooled down until the temperature measured by detector 2 reaches 125 K; the cryocooler is deactivated by the security system, and although the temperature continues decreasing, detector 2 does not reach the temperature limit defined at 120 K. In both cases, the temperature of the copper plate recovers the defined safe temperature level around 5 min later.[36]

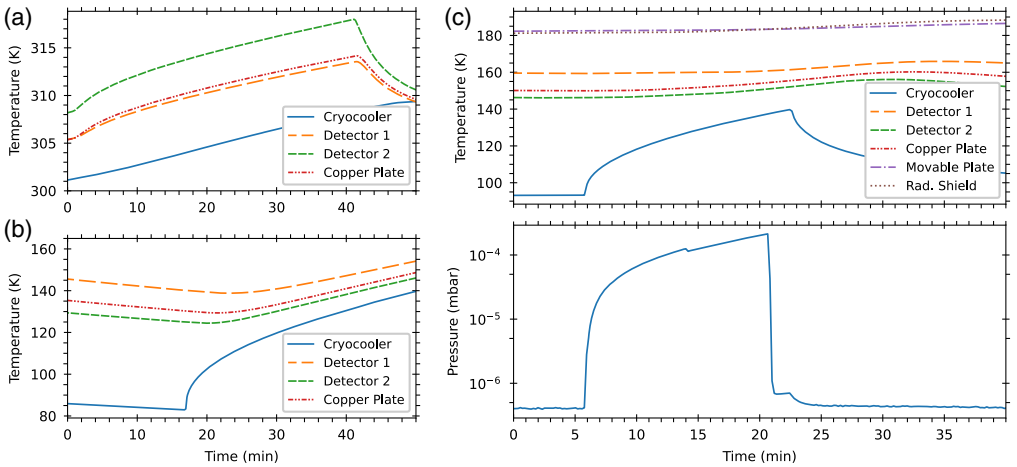

Fig. 8 Results from the most representative validation tests of the security system. No real detector was installed in the facility, but additional temperature sensors on the copper plate were used to reproduce the required thermometry signals to the security system. (a) High-temperature alarm test: temperature stops increasing due to the automatic disconnection of the heaters of the copper plate when detector 2 reaches 318 K. (b) Low-temperature alarm test: temperature stops decreasing due to the automatic disconnection of the cryocooler when detector 2 reaches 125 K. (c) Emergency stop button test: the pressure increases in the vacuum chamber due to the closing of the electro-pneumatic valve (bottom), followed by the increase of temperature at the mount due to the disconnection of the cryocooler (top); temperature and pressure decrease after some minutes due to the successful reactivation of the pumping system and the cryocooler. Alarm tests were repeated for each temperature sensor whose temperature limits were critical.

The results of the emergency stop button tests [Fig. 8(c)] are representative of those obtained from other tests, such as power blackout, leak detection, and failure of the pumping system. Each of them causes the closing of the electro-pneumatic valve and the deactivation of the cryocooler. In this case, the test started from the nominal vacuum level. A quick increase in pressure of about two orders of magnitude is observed after the closing of the electro-pneumatic valve. Shortly after, there is an increase in temperature due to the disconnection of the cryocooler, which in consequence produces outgassing that increases the pressure level of the vacuum chamber as well. If the vacuum level increases to 10^{-2} mbar, the turbopump can no longer be activated. However, no contamination is expected even if the detector returns to room temperature because as soon as the turbopump is activated again, the mount and the detector will release the trapped molecules during their passive warming-up, and once the cryocooler is activated these molecules will be trapped again by the cold head.[38] In case such an event takes place, a reaction time of less than an hour is expected from the personnel in charge of the facility.

3.2 Optical System

The validation of the optical system included the characterization of the stability of the QTH lamp, the photon flux under the different ND filters, the photon flux available per wavelength, the homogeneity of the IS at the optical WP, the transmission of the filter at the movable plate, and the level of straylight inside the radiation shield. The radiometric model of the facility[37] was essential to validate the results, especially to estimate the radiance at the output of each optical component of the facility coming from both the light source and the blackbody emissions of the individual optical surfaces.

The calibration of the power supply of the QTH lamp was verified in-house using a calibrated multimeter and a calibrated shunt load with 0.1 Ω resistance. The deviation between the current provided by the power supply of the QTH lamp and the measured value by the multimeter was ∼1.2%. However, since the QTH lamp is used in a relative scale, the calibration of its power supply is not critical.

The attenuation of the light source when passing through the two filter wheels of the facility was characterized at the IS level. Each filter wheel has 6 different positions where 9 ND filters are placed (optical densities from 0.17 to 2.3). The ND filters were selected in such a way that all cross combinations contribute to a uniform sampling of the illumination level, from the maximum flux to a flux lowered by 3 to 4 orders of magnitude,[34] reaching up to 30 different levels of attenuation at a certain wavelength. The analysis of the level of illumination is based on the ratio between the maximum flux at the selected wavelength (obtained from the OPEN position available) and the set of all other possible combinations, including the OPEN position. Since there is a variable level of available radiance at the viewport due to the spectrum of the light source and the wavelength-dependent transmission of the optical components, a slight change in a selected wavelength would provide a new set of 30 slightly different levels of illumination. Therefore, it can be considered that the VIS-NIR facility provides high tunability in terms of illumination. However, although the characterization performed provides information about the most appropriate combination of filters to be applied during measurements, the accurate attenuation that a detector is receiving should be characterized in real-time through the photodiodes located at the IS.

The optical power available at every output of the IS, useful for absolute radiometry, was measured with the calibrated photodiodes available (see Sec. 2.2). Figure 9 shows the spectral radiance available at the main output port of the IS for different BWs, as measured by the Si and PbS photodiodes. The relation between the optical power that the photodiode would receive at the WP and at the actual output port of the IS is given by a dimensionless transfer function R_0 determined by Eq. (1). The parameters S_{IS} and S_{WP} were experimentally acquired and constitute the net signal of the photodiode in A, as measured at the output of the IS and at the WP, respectively. R_0 also takes into account the ratio between the solid angles corresponding to the different geometries where the photodiode was located

$$R_0(\lambda) = \frac{S_{WP}(\lambda)}{S_{IS}(\lambda)}. \tag{1}$$

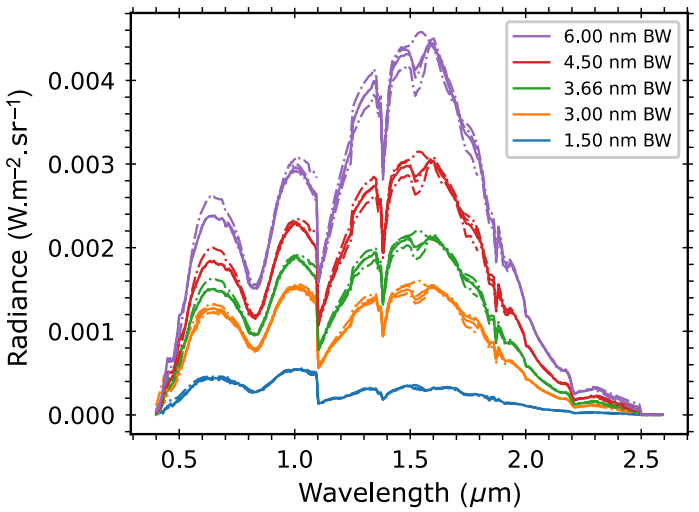

Fig. 9 Measurement of the spectral radiance produced by the 1000 W QTH lamp of the facility, and available at the main output port of the IS for different BWs.[37] The thick lines represent the average radiance whose measurements are represented by the dashed lines. The drop in radiance at 1.1 μm is due to the replacement of the Si photodiode by the PbS photodiode.

However, the illumination of the WP is not fully homogeneous. The flux homogeneity at the output of the IS was quantified by a calibrated photodiode coupled with a pinhole at the WP. The photodiode was used to scan the illumination from the IS at different wavelengths, passing through the baffle of the radiation shield inside the vacuum chamber, in steps of 2 mm. An inhomogeneity matrix was obtained by interpolating the measurements to get a finner grid that can be adapted to the pixel width of the detector to be characterized.[37] Since no significant spectral dependence was observed during the performed measurements (~2%), no spectral dependence is considered for radiance analysis during characterization campaigns.[34] The final inhomogeneity matrix of the IS (Fig. 10) is constituted by the average of the matrix as measured in the WP, generated by the output illumination of the IS for each wavelength, and normalized to one at the orthogonal intersection centered on the viewport. The homogeneity is especially high for the central part, describing a square of ~16 mm around the central pixel with a homogeneity close to one. The extremes of the matrix, excluding the corners, present a decrease of only 15%

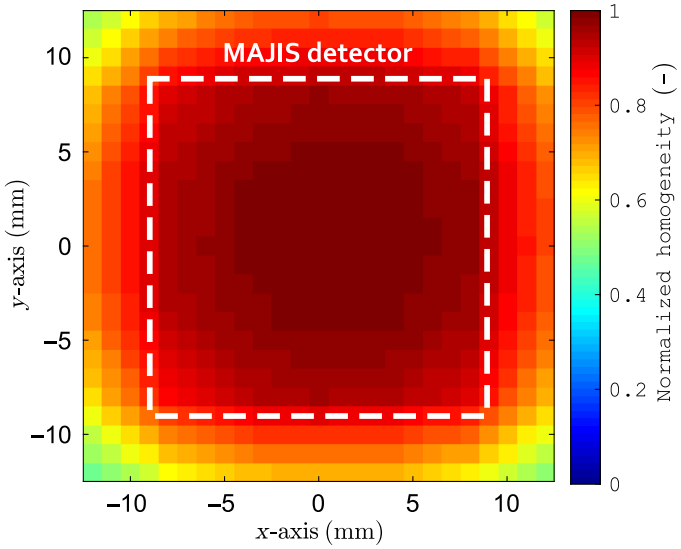

Fig. 10 Characterization of the homogeneity from the IS at the optical WP interpolated to 1 mm. The center position corresponds to the intersection with the optical axis. The white square represents the sensitive area of the MAJIS VIS-NIR detector.

with respect to the center. The remaining inhomogeneity encountered is considered for the estimation of the spectral power in the radiometric model as a multiplicative factor for all wavelengths. Therefore, the spectral power at a certain point in the WP $P_{\mathrm{WP}}(x, y, \lambda)$ is deduced by considering the net average spectral power as measured by the reference photodiode at the IS $P_{\mathrm{IS}}(x, y, \lambda)$, the homogeneity propagation function $H(x, y)$, and the transfer function $R_0(\lambda)$ as

$$P_{\mathrm{WP}}(x, y, \lambda) = P_{\mathrm{IS}}(x, y, \lambda) R_0(\lambda) H(x, y). \tag{2}$$

The QE of the detector $\mathrm{QE}(\lambda)$ is defined by Eq. (3), where E_p is the photon energy illuminating the detector in J, F_{WP} is the light signal as measured by the detector (DC already subtracted) in digital units (DU), g is the derived conversion gain in e^-/DU, and IT is the integration time in seconds at which the signal was measured. Note that an overestimation of the electronic conversion gain can be induced by interpixel capacitance,[39] which can lead to an overestimation of the QE. For the MAJIS VIS-NIR detectors, a factor of 0.93 is applied to the determined conversion gain to correct this effect[30]

$$\mathrm{QE}(x, y, \lambda) = \frac{E_p}{P_{\mathrm{WP}}(x, y, \lambda)} \cdot g \frac{F_{\mathrm{WP}}(x, y)}{\mathrm{IT}}. \tag{3}$$

Optical alignment is ensured by constraining the critical parts of the mount shown in Fig. 11. The mount itself mechanically constrains the three degrees of freedom present in rotation, since the assembly was performed using screws with conical heads and a calibrated torquemeter to guarantee consistency between the real mount and the optomechanical design, including the integration of the detector on the cold plate. The optical axis of the facility is defined as the orthogonal light path centered on the viewport of the vacuum chamber. During the alignment validation, the optical axis was identified by a laser beam, and the mount inside the vacuum chamber was aligned by means of a cross-hair installed on the baffle of the radiation shield. The vertical alignment is performed by the translation system of the mount supporting the optical breadboard. One of the three axes of rotation of the mount is constrained by keeping the frontal part of the optical breadboard in contact with the vacuum chamber. Therefore, the mount can slide against the wall of the vacuum chamber and be aligned to the viewport by two calibrated jigs

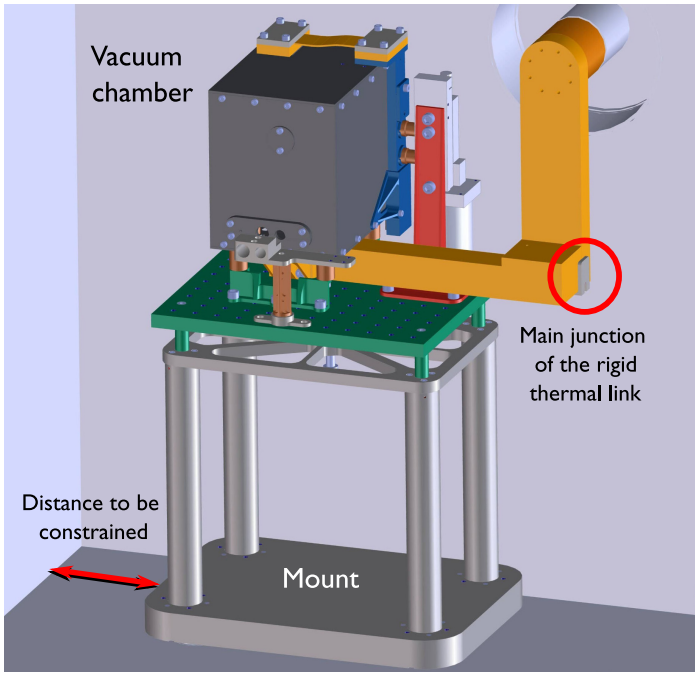

Fig. 11 Schematic view of the interior of the vacuum chamber. The red arrow on the left shows the linear distance constrained with a calibrated jig during alignment; the red circle on the right shows the main junction of the rigid thermal link constrained with an L-shape jig.

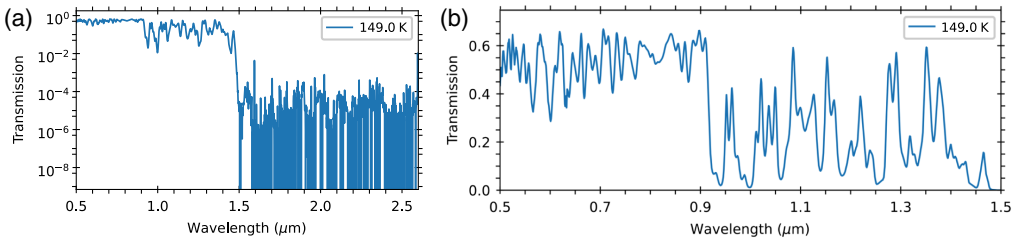

Fig. 12 Simulated transmission of the SWPF at nominal temperature: for the (a) whole spectral range of the BIRA-IASB facility and (b) spectral region below 1.47 μm.

manufactured as a result of this validation. This alignment procedure guarantees repeatability with a typical tolerance of 0.2 mm for translations.

The removal of thermal radiation above 1.47 μm is actually performed by two superposed short wave pass filters (SWPFs) at the movable plate of the radiation shield. The filters are customized by Northumbria Optical Coatings Ltd. The final flux transmission is observed in Fig. 12. Note that the SWPFs offer an average transmission of 54% between 0.4 and 0.9 μm but, despite the high rejection above 1.47 μm [Fig. 12(a)], only 16 wavelengths between 0.9 and 1.47 μm provide a transmission >30% [Fig. 12(b)]. This is the main limitation of the BIRA-IASB VIS-NIR facility (see Sec. 4). Therefore, the measured background signal from thermal emitters must be carefully subtracted during measurements. In addition, measuring QE will require considering windowing techniques or short integration times to avoid saturation of the detector at wavelengths above 1.47 μm. From modeling, the residual straylight from undesirable thermal emitters on the optical path was estimated to generate <10 $e^- pix^{-1} s^{-1}$ when using the SWPFs.

Measuring the level of straylight inside the radiation shield requires the mount at cryogenic temperatures and the detector under dark conditions, so the photon flux reaching the detector is only due to thermal emission around it. This validation was a process performed during the characterization campaigns of the MAJIS VIS-NIR detectors[31,38] and meant the improvements performed between campaigns. The main modifications from the original design were related to the baffling system of the slit of the movable plate and the main flexible thermal link between the movable plate and the radiation shield. A general improvement was also performed concerning the isolation between the movable plate and the translation stage, which must remain at a temperature above 250 K. As a result, the final level of straylight measured under dark conditions was finally negligible during the MAJIS SM campaign and allowed the straylight characterization inside the radiation shield of the mount.[31]

4 Comparison Against Other Facilities

The BIRA-IASB VIS-NIR characterization facility was developed to be a simple and versatile option for characterizing space-based detectors. Other characterization facilities were discussed in Sec. 1. Some clear advantages of the BIRA-IASB facility against some of them are discussed in this section.

4.1 Light Source

The selected light source is a QTH lamp of 1000 W, whose radiance is similar to a blackbody at 3200 K. This lamp provides enough flux not only to saturate the detector but also to persist with enough signal after passing by two ND filters, a double-monochromator, and an IS. In general, the power of the lamps used in other facilities[18,20,21,23] is not higher than 500 W. Moreover, the radiance stability of the BIRA-IASB lamp is 0.1%, which is better than the stability achieved by Crouzet et al.[18] (<1%) and Koshak et al.[19] (0.5 %). Although the spectral range of the QTH lamp covers ultraviolet to NIR wavelengths, the facility is used between 0.4 and 2.65 μm due to the gratings of the double-monochromator. Therefore, an upgrade to extend the wavelength range of the VIS-NIR facility is possible by replacing the gratings.

4.2 Double-Monochromator

The facility provides tunability of the VIS-NIR spectral wavelength range with bandpasses from 1 to 10 nm, thanks to the use of a double-monochromator. None of the facilities described in

Sec. 1.2 specifies the use of a double-monochromator to extract the required wavelength. Typically, when using a single-monochromator, additional filters shall be implemented to improve the purity of the signal, as is the case for Hill et al.,[27] Crouzet et al.,[18] and Coles et al.[23] The advantage of using a double-monochromator is to provide a tunable monochromatic flux with a high level of straylight rejection at the output selection; the undesirable high orders of diffraction are removed thanks to the internal filter wheel equipped with high-pass filters. Typically, the wavelength scale accuracy increases from ± 0.2 to ± 0.1 nm, when compared against a single-monochromator, and the wavelength reproducibility also increases from ± 0.05 to ± 0.025 nm.[40] After calibration, the wavelength scale accuracy of the facility was optimized using tabulated lines provided by spectral lamps between 0.4 and 3.5 μm.

Some test facilities directly illuminate the detector with LEDs for specific wavelengths, offering accuracy in the order of 5% to 10%, as observed in Rauscher et al.[16] However, although these facilities can perform measurements, such as linearity, they would be limited if a wide spectral range is required for measurements, such as QE. This is the reason why Secroun et al.[13] offer two configurations: one for specific measurements under LED sources, and one with a continuum wavelength range for QE measurements, including the use of a monochromator and a QTH lamp source.

4.3 Dynamical Illumination Levels

Similar to the BIRA-IASB facility, Cosentino et al.[26] use different ND filters to provide adjustable radiance, whereas facilities, such as Crouzet et al.,[18] prefer the use of apertures to vary the intensity of the flux. Another example is the case of Hill et al.[27] or Biesiadzinski et al.,[22] where the flux is decreased by varying both the size of a pinhole and the combination of ND filters. The BIRA-IASB facility combines ND filters in two filter wheels to reach up to 30 different levels of attenuation over four orders of magnitude, the same value as provided by Hill et al. In the BIRA-IASB facility, the ND filters were selected to contribute to a uniform sampling of the illumination level: a slight wavelength change offers a new set of 30 slightly different levels due to the spectral distribution of the QTH lamp combined with the transmissions of the spectrometer and the optical fiber, providing in consequence a great tunability in terms of illumination.

The use of two linear polarizers, from aligned- to cross-orientation, could provide different but continuous levels of illumination. This is another solution to be explored in a later upgrade. The IS would remove polarization features, but special attention should be paid to the cooling system dedicated to the optics at the light entrance level, since the 1000 W lamp can provide an optical power larger than the threshold limit and could damage the polarizers.

4.4 Absolute Radiometry

Thanks to the homogeneity characterization of the light flux at every point of the WP (1 mm steps, see Sec. 3.2), the IS can directly illuminate the detector to perform absolute radiometry, with continuous monitoring of the light flux during data acquisition. Facilities, such as Christov et al.,[20] Weatherill et al.,[21] Coles et al.,[23] and Serra et al.,[4] include a ~ 1 m long baffle between the output port of the IS and the WP, to reduce straylight and increase uniformity despite sacrificing intensity. In the BIRA-IASB facility, the detector is aligned as close as possible to the output port of the IS outside the vacuum chamber (86 mm from the viewport). Straylight is decreased by the cold baffle of the radiation shield, and beam stability is monitored in real-time by calibrated InGaAs and PbS/Si photodiodes installed in the additional output ports of the IS. Other facilities, such as Crouzet et al.,[18] implement a pick-up mirror to either focus the light on the detector under test or on the reference photodiode when necessary, so no monitoring in real-time is possible. Another example is Biesiadzinski et al.,[22] where a 70/30 beam splitter is used instead to provide feedback to the reference photodiode while illuminating the detector to be characterized. Therefore, continuous monitoring is possible at the cost of decreasing flux, which is not desirable when using a 50 W lamp. In any case at the BIRA-IASB facility, the accurate alignment of the detector with respect to the IS is critical.

4.5 Cryogenic Capabilities

The BIRA-IASB facility uses a closed-cycle cryostat with one single cold head to thermalize the detector and the radiation shield at cryogenic temperatures. Some facilities, such as Crouzet et al.[28]

and Biesiadzinski et al.,[22] still prefer the use of open-cycle cryostats mainly due to the absence of vibrations from the pumping and cryogenic systems that can affect the stability of the detector under test. The clear disadvantage is the periodic refill of the cryostats unless it is performed automatically, as in Weatherill et al.[21] This is not an issue for the BIRA-IASB facility, since the detector mount was mechanically designed to compensate for any vibration from the cryogenic system. Another disadvantage of the open-cycle cryostats is the minimum temperature achievable by these systems. Typically based on the use of liquid nitrogen (LN2), they do not reach temperatures lower than 120 K, whereas the BIRA-IASB facility is able to thermalize detectors from 50 to 382 K with a maximum temperature rate of -0.9 K/ min, a rate comparable to facilities, such as Crouzet et al.[28] and Weatherill et al.[21] The copper plate is able to stabilize within 0.01 % of the target temperature, with a precision better than 7 mK.

When part of the optical system is also thermalized at cryogenic temperatures, two-stage cold head systems are preferred, as is the case for the Teledyne Imaging Sensors Test Facility,[16] the Independent Detector Testing Laboratory,[24] and the University of Hawaii Test Facility.[29] The disadvantage of only thermalizing the detector and its surrounding radiation shield at cryogenic temperatures is visible in NIR measurements. Then, the thermal contribution of the viewport of the vacuum chamber and any object behind it within the field of view of the detector must be removed. The facilities, which typically thermalize optical components inside the cryostats, cover wavelengths above 2.0 μm. Since the BIRA-IASB facility covers a spectral range up to 2.65 μm, the approach is similar to that of Crouzet et al.,[18] with the use of a cold SWPF to remove the emission of warm objects outside the vacuum chamber at wavelengths longer than 1.47 μm.

4.6 Remote Control

Thanks to the design of the BIRA-IASB facility, typical detector characterization measurements requiring dark conditions, different temperatures, and dynamical illumination levels and wavelengths can be performed in one single cooling cycle without the need of changing the configuration of the setup, which ensures the repeatability of measurements. Especially for dark conditions, some facilities, such as Serra et al.,[4] perform measurements with a lid on the detector and, after a second cooling cycle, perform measurements under light conditions with the lid removed. The LabVIEW-based GSE allows the remote control of both the optical system and the cryogenic system without the need of accessing the clean area where the facility is installed, except for the manual adjustment of the width of the variable slits of the monochromator. Therefore, most of the processes can be automatized, including the pumping and cooling-down and measurements that do not need the adjustment of the variable slits. This is also the case for facilities, such as Crouzet et al.,[18] Secroun et al.,[13] and Christov et al.[20]

The BIRA-IASB facility was designed to characterize one detector at a time. If the current configuration of the mount is not modified, the size of a detector unit must be less than 138.5 mm $\times$ 106 mm $\times$ 111.5 mm to fit inside the radiation shield of the facility. Other facilities allow the characterization of multiple detectors in a single cooling cycle, including mosaics, although depending on the optical configuration it might be required to perform different cooling cycles to perform measurements at other optical configurations. Some examples are the ultra low background[29] and the Teledyne Imaging Sensors[16] test facilities.

It is worth mentioning that the possibility of remote control and performing automatized measurements is also possible due to the robust security system developed for the BIRA-IASB facility. In this way, the facility can keep the detector under cryogenic conditions for several weeks, whereas ensuring protection against thermalization outside the operating range, vacuum loss, and electric failures.

4.7 Other Measurements

Although the BIRA-IASB facility was developed to perform relative and absolute irradiance measurements at the detector plane, some specialized measurements are not possible to perform in the current configuration, including modulation-transfer-function (MTF), pixel spot scanning, charge transfer efficiency (CTE), and pulse illumination. The pixel spot scanning feature has been used in other facilities, such as Crouzet et al.,[18] as a second method to measure QE in combination with a collimated light beam. However, in the BIRA-IASB facility, the QE is

measured directly from the exposure to the well-characterized flux of the IS, and it was not necessary to develop a scanning system for this purpose. In any case, a non-vacuum-compatible scanning system is available at the laboratory if required. This was used for characterizing the homogeneity of the IS at the optical WP and could be adequate to become a proper pixel spot scanning in the future. Implementing the possibility to perform MTF and CTE measurements would require the inclusion of a movable knife-edge close to the detector and a ^{55}Fe light source to provide high-energy photons.

In addition, the modularity of both the optical and cryogenic systems allows their use independently. This can be appreciated for the characterization of VIS-NIR detectors with no cryogenic requirements demanded, or if thermal testing of electronic devices is necessary.

Radiation testing is out of the scope of the BIRA-IASB facility, and would require the use of radioactive sources, such as Ruthenium 106 or Chlorine 36, and a different type of viewport. Moreover, only other than flight or spare detectors would be exposed to these tests. For the MAJIS VIS-NIR detectors, the effect of high-energy electrons impacting their sensitive area was investigated by the Liege Space Center.[41]

5 Conclusions

The BIRA-IASB VIS-NIR facility is a single versatile test bench developed to perform absolute radiometric measurements for characterizing space-based detectors. The facility is in a certified ISO-5 environment compliant with ESCC and EMVA standards, with continuous monitoring of temperature, pressure, and relative humidity, and is provided with active systems to control temperature and humidity. The optical system allows the acquisition of data under dark conditions with straylight levels leading to <10 e^- pix^{-1} s^{-1}. Monochromatic light flux is provided in the spectral range between 0.4 and 2.65 μm, with straylight rejection of 10^{-8}, high radiance stability ($\sim$0.1%), and wavelength accuracy of $\pm$0.1 nm,[40] tunable from 1 to 10 nm BW. Moreover, the facility provides up to 30 different levels of illumination per wavelength at the WP. In this facility, the output port of the IS directly illuminates the detector's sensitive area inside the vacuum chamber. Thanks to the calibration of the spectral power at the WP and the repeatability ensured for optical alignment (<0.2 mm), it is possible to perform absolute radiometry and measure QE.

Concerning the thermal-vacuum performances of the facility, the ultimate pressure of the system is in the order of 10^{-7} mbar, although it is possible to achieve 10^{-5} mbar after 80 min of pumping. Then, the closed-cycle cryocooler can be activated to thermalize the copper base plate with a maximum cooling rate of 0.9 K/min. The vacuum chamber has a capacity of 420 L and counts with redundant gauges and overpressure relief valves for safety reasons. In addition, six PID temperature control loops are available at the facility, each of them with the possibility of configuring alarms dedicated to the protection of sensitive devices; up to 24 temperature sensors can be monitored in real-time. The systematic error of the temperature measurements is expected to vary from 22 to 79 mK, depending on the temperature being measured.

In its current configuration, the BIRA-IASB facility can allocate one VIS-NIR detector unit inside the radiation shield of up to 138.5 mm $\times$ 106 mm $\times$ 111.5 mm and thermalize it with a stability better than 7 mK between 50 and 382 K. It is not required to open the vacuum chamber to modify its optical configuration. The cold radiation shield includes a movable plate that allows light flux to reach the detector if needed. In addition, it includes a SWPF that can be used to remove the thermal radiation from the viewport of the chamber and other warm objects on the optical path ($>$1.47 μm) to perform measurements at specific wavelengths. This is the main limitation of the BIRA-IASB facility. When using the filter, only 16 peak wavelengths can be used between 0.9 and 1.47 μm for QE measurements, when ideally, part of the optics should be also thermalized to allow a continuum sampling of the pixels response.

The BIRA-IASB facility can run continuously over several weeks and be remotely controlled by the GSE systems. It is not necessary for the operators to work in the clean area during the campaign of measurements. Depending on the needs of the user, the measurements can be performed manually or automatically. The only element that must be manually adjusted is the width of the variable slits of the double-monochromator to tune the bandpass to the required settings; these can be replaced by motorized slits in a future stage of the facility. Moreover, a robust security system was implemented to protect the detector and other sensitive devices

inside the vacuum chamber from the risk of damage due to temperatures outside their operating range, contamination due to failures in the vacuum system, and general electric failure, especially during non-working hours.

The BIRA-IASB VIS-NIR characterization facility was already used to characterize the SM and FM VIS-NIR detectors of MAJIS/JUICE,[30,31] and is now offered to the scientific community as another option for future characterizations.

Availability Statement

Data sharing is not applicable to this paper, as no new data were created or analyzed.

Acknowledgments

This project acknowledges the strong support provided by the Insitute d'Astrophysique Spatiale (IAS) in the development of the BIRA-IASB VIS-NIR characterization facility to comply with the requirements for the characterization of the MAJIS/JUICE VIS-NIR detectors, especially during the validation phase. In addition, we acknowledge the technical support provided by the Belgian User Support and Operation Center (BUSOC), which played an important role in certifying the activities performed. The Centre National d'Etudes Spatiales (CNES) is worthy thank for the knowledge transfer for the development of the security system. This project acknowledges funding by the (1) Belgian Science Policy Office (BELSPO) through PRODEX-11 project proposal "Characterization of JUICE/MAJIS VIS-NIR detectors" (Grant No. PEA 4000124255), (2) ESA JUICE project, and (3) Scientific Research Fund (FNRS) through (Grant No. 34828772) "MAJIS detectors and impact on science." S.R. and C.L. acknowledge additional funding by BELSPO through the FED-tWIN program (Prf-2019-077-RT-MOLEXO).

References

1. C. A. Shapiro et al., "Precision Projector Laboratory: detector characterization with an astronomical emulation testbed," *J. Astron. Telesc. Instrum. Syst.* **5**(4), 041503 (2019).
2. A. BenMoussa et al., "On-orbit degradation of solar instruments," *Sol. Phys.* **288**(1), 389–434 (2013).
3. J. R. Janesick, Ed., *Scientific Charge-Coupled Devices*, SPIE Press (2001).
4. B. Serra et al., "Characterization of Euclid-like H2RG IR detectors for the NISP instrument," *Proc. SPIE* **9602**, 167–180 (2015).
5. T. S. Lomheim, L. W. Schumann, and S. E. Kohn, "Experimental characterization, evaluation, and diagnosis of advanced hybrid infrared focal plane array electro-optical performance," *Proc. SPIE* **3379**, 520–554 (1998).
6. U. Jain, "Characterization of CMOS image sensor," Master's thesis, Delft University of Technology, Delft, Netherlands (2016).
7. G. Orias, "Accurate, high-throughput, low-cost testing of infrared focal plane arrays for defense-related systems," *Proc. SPIE* **2474**, 265–273 (1995).
8. J. D. Vincent et al., *Fundamentals of Infrared and Visible Detector Operation and Testing*, 2nd ed., John Wiley & Sons (2015).
9. P. Verhoeve et al., "CCD characterization for astronomy space missions at ESA," *Proc. SPIE* **9154**, 915416 (2014).
10. European Space Agency (ESA), "Optics and Opto-Electronics Laboratory," 2022, https://technology.esa.int/lab/optics-and-opto-electronics-laboratory
11. Goddard Space Flight Center, "Detector Characterization Laboratory," 2010, https://detectors.gsfc.nasa.gov/DCL/index.php
12. P. Verhoeve et al., "ESA's CCD test bench for the Euclid visible channel," *Proc. SPIE* **8453**, 845322 (2012).
13. A. Secroun et al., "Characterization of H2RG IR detectors for the Euclid NISP instrument," *Proc. SPIE* **9915**, 649–657 (2016).
14. D. F. Figer et al., "Independent testing of JWST detector prototypes," *Proc. SPIE* **5167**, 270–301 (2004).
15. D. N. B. Hall et al., "Performance of the first science grade $\lambda c = 2.5$ μm HAWAII 4RG-15 array in the laboratory and at the telescope," *Proc. SPIE* **9915**, 99150W (2016).
16. B. J. Rauscher et al., "Detectors for the James Webb Space Telescope near-infrared spectrograph. I. Readout mode, noise model, and calibration considerations," *Publ. Astron. Soc. Pac.* **119**(857), 768 (2007).
17. I. V. Kotov et al., "Characterization and acceptance testing of fully depleted thick CCDs for the large synoptic survey telescope," *Proc. SPIE* **9915**, 99150V (2016).
18. P. E. Crouzet et al., "Quantum efficiency test set up performances for NIR detector characterization at ESTEC," *Proc. SPIE* **9154**, 91541G (2014).

19. W. J. Koshak et al., "Laboratory calibration of the optical transient detector and the lightning imaging sensor," *J. Atmos. Ocean. Technol.* **17**(7), 905–915 (2000).
20. A. Christov et al., "Test stand for characterization of optical sensors for astronomy," *J. Astron. Telesc. Instrum. Syst.* **5**(4), 041504 (2019).
21. D. P. Weatherill et al., "An electro-optical test system for optimising operating conditions of CCD sensors for LSST," *J. Instrum.* **12**(12), C12019 (2017).
22. T. Biesiadzinski et al., "Measurement of reciprocity failure in near-infrared detectors," *Publ. Astron. Soc. Pac.* **123**(900), 179 (2011).
23. R. Coles et al., "An automated system to measure the quantum efficiency of CCDs for astronomy," *J. Instrum.* **12**(04), C04014 (2017).
24. D. F. Figer et al., "Independent detector testing laboratory and the NGST detector characterization project," *Proc. SPIE* **4850**, 981–1000 (2003).
25. N. Bezawada et al., "Characterisation activities of new NIR to VLWIR detectors from Selex ES Ltd. at the UK ATC," *Proc. SPIE* **9154**, 91540O (2014).
26. R. Cosentino et al., "Laboratory test of the VIS detector system of SOXS for the ESO-NTT Telescope," *Proc. SPIE* **12184**, 121845I (2022).
27. R. J. Hill et al., "Reciprocity failure in 1.7 μm cut-off HgCdTe detectors," *Proc. SPIE* **7742**, 774222 (2010).
28. P. E. Crouzet et al., "Test set up description and performances for HAWAII-2RG detector characterization at ESTEC," *Proc. SPIE* **8453**, 845329 (2012).
29. D. N. B. Hall et al., "A 4 K × 4 K HgCdTe astronomical camera enabled by the JWST NIR detector development program," *Proc. SPIE* **5499**, 1–14 (2004).
30. P. Haffoud et al., "MAJIS VIS-NIR channel: performances of the focal plane unit - flight model," *Proc. SPIE* **12180**, 1218039 (2022).
31. N. Pereira et al., "MAJIS VIS-NIR channel: performances of the spare model focal plane unit," *Proc. SPIE* **12180**, 121803I (2022).
32. European Space Components Coordinator, "Electro-optical test methods for charged coupled devices," ESCC Basic Specification No. 25000, European Space Agency (2014).
33. European Machine Vision Association, "EMVA Standard 1288: standard for characterisation of image sensors and cameras," Release 3.1, European Space Agency (2016).
34. D. Bolsée et al., "Characterization facility for the MAJIS/JUICE VIS-NIR FM and SM detectors," *Proc. SPIE* **11443**, 114437H (2020).
35. PAR Group Ltd., SSUSTAPEI, Technical datasheet (2020).
36. M. E. Cisneros-González et al., "Thermal-vacuum and security system of the characterization facility for the MAJIS/JUICE VIS-NIR FM and SM detectors," *Proc. SPIE* **11443**, 114437G (2020).
37. L. V. Laeken, "Development of experimental benches for radiometric characterization: application to space instrument MAJIS VIS-NIR on JUICE," Master's thesis, Université de Liège, Liège, Belgium (2019).
38. M. E. Cisneros-González et al., "MAJIS/JUICE VIS-NIR FM and SM detectors characterization," *Proc. SPIE* **11443**, 114431L (2020).
39. S. Seshadri et al., "Mapping electrical crosstalk in pixelated sensor arrays," *Proc. SPIE* **7021**, 702104 (2008).
40. Bentham Instruments Limited, "DTMc300 double-monochromator with triple grating turret," 2023, https://www.bentham.co.uk/products/components/dtmc300-double-monochromator-39/
41. P. Guiot et al., "Characterization of transient signal induced in IR detector array by Jupiter high-energy electrons and implications for JUICE/MAJIS operability," *Planet. Space Sci.* **181**, 104782 (2020).

Miriam E. Cisneros-González received her BS degree in electronics engineering from Durango Institute of Technology (ITD) and her MS degree in astrophysics from National Institute of Astrophysics, Optics and Electronics (INAOE) in Mexico. She is a PhD candidate under the supervision of C.L. and S.R. since 2018. She has participated in the development of different astronomical instruments, mainly related to VIS-NIR spectrometers. Her current research interests include the study of giant planets' atmospheres.

David Bolsée received his MS degree and PhD in physics and geophysics from Free University of Brussels in 1989 and 2012, respectively. He has worked at the Royal Belgian Institute for Space Aeronomy (BIRA-IASB) for 33 years. He gained expertise in optical metrology, radiometry, and solar spectral irradiance measurements. He was Principal Investigator of the SOLAR/SOLSPEC Mission on ISS (between 2008 and 2017) and is currently head of the Belgian Radiometric Laboratory (B.RCLab) and responsible for the development of the BIRA-IASB characterization facility.

Nuno Pereira received his MS degree in physics engineering from Technical University of Lisbon. He started at the BIRA-IASB working with SOLAR/SOLSPEC data. Later, he was

involved in the radiometric characterization of the MAJIS/JUICE VIS-NIR detectors. He is currently a PhD candidate working on VenSpec-H/EnVision, analyzing the impact of the instrumental features on science, extending radiative transfer models to Venus-like exoplanets, and tackling some of the science questions.

Lionel Van Laeken has been working since 2018 at the BIRA-IASB on the ESA JUICE mission to Jupiter. His team was responsible for the spectral characterization of the flight and spare models of the MAJIS spectrometer, payload of the JUICE satellite. During his 4-year career at BIRA-IASB, he participated in the development of a test facility to reproduce Jupiter's environment to correctly calibrate the MAJIS VIS-NIR detectors.

Lars Jacobs received his MS degree in electromechanics in 2014. He started in the pharmaceutical industry as software validation engineer but soon realized that his passion lay more in the creativity of mechanical design. He joined the BIRA-IASB in 2016 as mechanical project engineer, supporting many ground and space instruments, such as 3DEES (Proba-3), VenSpec-H (EnVision), and MAJIS (JUICE). He is now head of the Department of Mechanics at BIRA-IASB.

Ann Carine Vandaele is the head of the Solar Radiation in Atmospheres Division at the BIRA-IASB. She has been PI of SOIR/VEx and NOMAD/ExoMars Trace Gas orbiter, and is currently PI of the future VenSpec-H/EnVision instrument. She is also co-I of MAJIS/JUICE. She is a member of the JWST Mars Focus Group. Her main scientific expertise lies in the development of space instruments, spectroscopy, and radiative transfer modeling.

Özgür Karatekin is a senior research scientist at the Royal Observatory of Belgium (ROB). Since 2001, he has been working on planetary sciences. He takes active part in several space missions including ESA's ExoMars (NOMAD (co-I)), (AMELIA (co-PI)), HERA (JUVENTAS/GRASS (PI)), and JUICE (MAJIS (co-I)). His main scientific expertise lies in planetary atmosphere surface interactions, geophysics, and geodesy. His research interests include the study of ices, organics, and minerals of the Jupiter's icy moons.

Clément Lauzin leads a research group in the Institute of Condensed Matter and Nanosciences of Université Catholique de Louvain (UCLouvain). His group specialized in the building of high-resolution and high-sensitivity spectrometers, besides the use of advanced techniques to cool down molecules to a few Kelvin. The measurements performed with those instruments are relevant for astrophysics and planetary studies and ultimately lead to the understanding of the considered molecular spectral signature.

Séverine Robert is a staff senior scientist in the Planetary Atmospheres Unit at the BIRA-IASB, Belgium. Her background is in infrared spectroscopy and radiative transfer modeling. First as a scientist (SOIR/Venus Express and NOMAD/ExoMars TGO), then as a project manager of the VenSpec-H instrument onboard EnVision, she acquired expertise in instrumental and mission development. She is an instrument scientist of VenSpec-H and is involved in various missions (Ariel, JUICE).